Journal of Computational Physics **175,** 674–701 (2002)
doi:10.1006/jcph.2001.6962, available online at http://www.idealibrary.com on IDEAL®

Hybrid Flux-Splitting Schemes for a Two-Phase Flow Model

Steinar Evje and Kjell K. Fjelde

RF-Rogaland Research, Thormøhlensgt. 55, N-5008 Bergen, Norway
E-mail: steinar.evje@rf.no, kjell-kaare.fjelde@rf.no

Received March 23, 2001; revised October 15, 2001

In this paper we deal with the construction of hybrid flux-vector-splitting (FVS) schemes and flux-difference-splitting (FDS) schemes for a two-phase model for one-dimensional flow. The model consists of two mass conservation equations (one for each phase) and a common momentum equation. The complexity of this model, as far as numerical computation is concerned, is related to the fact that the flux cannot be expressed in terms of its conservative variables. This is the motivation for studying numerical schemes which are not based on (approximate) Riemann solvers and/or calculations of Jacobian matrix. This work concerns the extension of an FVS type scheme, a Van Leer type scheme, and an advection upstream splitting method (AUSM) type scheme to the current two-phase model. Our schemes are obtained through natural extensions of corresponding schemes studied by Y. Wada and M.-S. Liou (1997, *SIAM J. Sci. Comput.* **18**, 633–657) for Euler equations. We explore the various schemes for flow cases which involve both fast and slow transients. In particular, we demonstrate that the FVS scheme is able to capture fast-propagating acoustic waves in a monotone way, while it introduces an excessive numerical dissipation at volume fraction contact (steady and moving) discontinuities. On the other hand, the AUSM scheme gives accurate resolution of contact discontinuities but produces oscillatory approximations of acoustic waves. This motivates us to propose other hybrid FVS/FDS schemes obtained by removing numerical dissipation at contact discontinuities in the FVS and Van Leer schemes.

Key Words: two-phase flow; hyperbolic system of conservation laws; flux-vector splitting; flux-difference splitting; hybrid scheme; numerical dissipation.

1. INTRODUCTION

A recent trend in the development of upwind schemes has been to construct hybrid flux-difference-splitting (FDS) and flux-vector-splitting (FVS) schemes where one tries to combine the accuracy of FDS in the resolution of contact discontinuities and the robustness

0021-9991/02 $35.00

of FVS in the capturing of stronger discontinuities. For an overview of different implementations of such ideas for calculation of single-phase inviscid flow (Euler equations) as well as viscous flow (Navier–Stokes) we refer to [7] and references therein. The purpose of this work is to explore such approaches for a two-phase model used to simulate unsteady compressible liquid and gas flow in pipes.

The unsteady two-phase simulation represents an important tool for gaining insight into flow processes where oil and gas are transported simultaneously out of a reservoir. To design and operate such transport systems, flow rate and pressure fluctuations must be predicted with good accuracy. Such fluctuations typically arise due to a combination of operating conditions and the two-phase nature. The two-phase model we explore in this work is written in the following conservative vector form:

$$\partial_t \begin{pmatrix} \alpha_l \rho_l \\ \alpha_g \rho_g \\ \alpha_l \rho_l v_l + \alpha_g \rho_g v_g \end{pmatrix} + \partial_x \begin{pmatrix} \alpha_l \rho_l v_l \\ \alpha_g \rho_g v_g \\ \alpha_l \rho_l v_l^2 + \alpha_g \rho_g v_g^2 + p \end{pmatrix} = \begin{pmatrix} 0 \\ 0 \\ -q \end{pmatrix}. \tag{1}$$

The model assumes isothermal conditions, and the unknowns are ρ_l, ρ_g the liquid and gas densities, α_l, α_g the volume fractions of liquid and gas, v_l, v_g the velocities of liquid and gas, p the common pressure for liquid and gas, and q a source term. The system is a one-dimensional two-phase model of the drift-flux type. Since the momentum is given only for the mixture, we need an additional closure law, a so-called hydrodynamic closure law, which connects the two-phase velocities. More generally, this law should be able to take into account different flow regimes. In addition, we need a thermodynamic equilibrium model which specifies the fluid properties. For more details related to the current two-phase model we refer to [1, 9, 10, 17, 20].

Due to the complexity of the hydrodynamic and thermodynamic models, we cannot expect to have an analytical expression for the physical flux $F(\mathbf{w})$ associated with Eq. (1) in terms of its conservative variables $\mathbf{w}$ [9, 15, 17]. In general, it is therefore difficult to use more classical numerical schemes such as the Godunov or Roe schemes which are based on an algebraic given Riemann solver. For works dealing with numerical schemes for the present two-phase model we refer to Masella *et al*. [15], Romate [17], Faille and Heintze [9], Fjelde and Karlsen [11], and Evje and Fjelde [8]. The crucial point is that we have no analytical expression for the Jacobian matrix, hence this must generally be computed numerically. Therefore, the potential gain in terms of computation time by using sequential-based methods like hybrid FVS/FDS schemes becomes a much more important aspect for the current two-phase model than for the Euler equations. This fact has been a main motivation for exploring how to extend hybrid FVS/FDS type discretization techniques to the present two-phase model. Through these investigations we also seek to obtain insight into discretization techniques that can be applied to more general two-phase models as well, i.e. two-fluid models where a set of equations for each phase must be considered.

At this point we recall some general facts regarding FVS versus FDS schemes. Up to now several basic upwind schemes have been proposed, and most of them are categorized as either FDS or FVS. The former is based on using an exact or approximate solution of the local Riemann problem, while the latter typically splits the flux vector into upstream and downstream traveling components according to the sign of its eigenvalues. More precisely, in FVS, the flux function F is divided into positive and negative parts,

$$F(\mathbf{w}) = F^-(\mathbf{w}) + F^+(\mathbf{w}),$$

which give the numerical flux at the cell interface $(j + 1/2)$ between the states $\mathbf{w}_L$ and $\mathbf{w}_R$ by considering

$$F_{j+1/2}(\mathbf{w}_L, \mathbf{w}_R) = F^+(\mathbf{w}_L) + F^-(\mathbf{w}_R). \tag{2}$$

FDS is based on matrix calculations, while FVS is based on scalar calculations. Consequently, FVS is more efficient than FDS; however, it introduces excessive numerical dissipation. During the past few years much of research has been done on the Euler equations motivated by the desire to combine the efficiency of FVS and the accuracy of FDS. The idea is to eliminate surplus dissipation of the FVS by introducing the flavor of the FDS into FVS schemes. These schemes are not FVS anymore since their numerical flux typically cannot be expressed in the splitting form (2). They are a hybrid of FVS and FDS. We refer to [24] and [7] for nice overviews of different FDS and FVS schemes as well as hybrid FVS/FDS schemes studied for the Euler and Navier–Stokes equations.

In this paper we are interested in extending some flux-splitting schemes previously investigated for Euler and Navier–Stokes calculations to solve for unsteady compressible liquid and gas flow in a pipe. In particular, we consider the performance of an FVS type scheme, a Van Leer type scheme, and an advection upstream splitting method (AUSM) type scheme for the current two-phase model. Our schemes are obtained through natural extensions of corresponding single-phase schemes proposed by Wada and Liou [24] for Euler equations. We demonstrate that FVS is able to capture propagation of stronger discontinuities in a monotone way, while it introduces an excessive numerical dissipation at volume fraction contact (steady and moving) discontinuities. AUSM, on the other hand, gives accurate resolution of contact discontinuities, but produces highly oscillatory approximations for stronger discontinuities. This motivates us to propose other hybrid FVS/FDS schemes obtained by removing dissipation in the FVS and Van Leer schemes at contact discontinuities.

One such approach is based on modifying the velocity-flux-splitting formulas associated with these schemes such that they yield vanishing numerical dissipation for a stationary volume fraction contact discontinuity while they produce a mass flux similar to that of AUSM for a moving volume fraction contact discontinuity. This idea is explored for the FVS and Van Leer schemes and gives rise to two corresponding schemes denoted as AUSMV and AUSMD (motivated by the notation used in [24]).

The rest of this paper is organized as follows: In Section 2 we give a more detailed presentation of the two-phase model we want to solve. In Section 3 we present three different flux-splitting schemes for the two-phase model, an FVS, a Van Leer and an AUSM type scheme. In Section 4 we consider the performance of these schemes for three different flow cases. We make some observations concerning the dissipation mechanism of the various schemes in Section 5. Then, in Section 6 we suggest an approach for removing excessive dissipation. Finally, in Section 7 we revisit flow cases studied in Section 4 and do more testing of the AUSMV scheme.

2. THE TWO-PHASE MODEL

The numerical simulation of two-phase flow is a challenging mathematical and industrial research area. The complete local description of such flows is very complex and an averaging technique is used to derive models suitable for computation [6, 13]. When motions of

the two phases are strongly coupled, the relative velocity of the two-fluid system is small and a simplified model can be obtained which consists of a system of conservation laws for the mass, momentum, and energy balance equations for the gas–liquid mixture. However, such mixture models (homogeneous equilibrium models) are inefficient when the kinematic disequilibrium becomes significant. For such cases a set of equations for each phase must be considered, which leads to so-called two-fluid models. Significant research activity related to the study of upwind type schemes and their extensions to different variants of the two-fluid model has taken place over the last 10 years; see [2–4, 5, 12, 18, 21, 22] and references therein.

For isothermal flow, one version of the basic one-dimensional two-fluid system is the following model:

$$\begin{aligned}
\partial_t[\alpha_l\rho_l] + \partial_x[\alpha_l\rho_l v_l] &= \Gamma_l \\
\partial_t[\alpha_g\rho_g] + \partial_x[\alpha_g\rho_g v_g] &= \Gamma_g \\
\partial_t[\alpha_l\rho_l v_l] + \partial_x\left[\alpha_l\rho_l v_l^2\right] + \alpha_l\partial_x p + \tau_l &= M_l^D + q_l \\
\partial_t[\alpha_g\rho_g v_g] + \partial_x\left[\alpha_g\rho_g v_g^2\right] + \alpha_g\partial_x p + \tau_g &= M_g^D + q_g.
\end{aligned} \tag{3}$$

The unknowns are ρ_l, ρ_g the liquid and gas densities, α_l, α_g the volume fractions of liquid and gas, v_l, v_g the velocities of liquid and gas, and p the common pressure for liquid and gas. Γ_l, Γ_g represent mass exchanges between the two phases, q_l, q_g are source terms representing frictional and gravity forces, while $M_l^D = -M_g^D$ are source terms reflecting interphase drag. Finally, τ_l, τ_g are differential terms which are mathematically relevant because they affect the well-posed nature of the system.

The above system is difficult to solve for several reasons: First, the system is not in conservation law form due to the pressure terms, and these terms must be carefully handled in the presence of discontinuities, (see [5] for instance). Second, the source terms associated with interphase drag are stiff, acting on a very short time scale. Typically, this can cause problems in the numerical computation [16]. Third, upwinding requires some knowledge of the eigenstructure of the Jacobian of the flux function corresponding to the above system. In contrast to the case of single-phase and two-phase mixture flow models, it is much more complicated to compute the eigenvalues and eigenvectors of the system due to complex phasic interactive processes [2, 4, 5]. Finally, we should mention that the system might fail to be hyperbolic. This can lead to an ill-posed problem which in turn might produce oscillations in the numerical solutions.

Two-phase flow models are widely used within the petroleum industry to describe production and transport of oil and gas through long pipelines as well as to evaluate the transient responses of drilling operations. Due to the complexity of the two-fluid model, modelers commonly use the simpler drift-flux model. This model is obtained from the two-fluid model by adding together the respective liquid and gas momentum and energy equations to produce mixture momentum and energy equations. Difficult terms related to phase interactions cancel out, and the missing information is replaced by an empirical slip equation which gives a relation between the phase velocities. Source terms related to mass transfer, friction, and gravity are still present in the model. In addition, the equations are now in conservative form. The drift-flux model has been shown to be hyperbolic, at least in a physically reasonable region of parameters [1, 17]. In particular, for isothermal flow, the

drift-flux model takes the form

$$\begin{aligned} \partial_t[\alpha_l\rho_l] + \partial_x[\alpha_l\rho_l v_l] &= \Gamma_l \\ \partial_t[\alpha_g\rho_g] + \partial_x[\alpha_g\rho_g v_g] &= \Gamma_g \\ \partial_t[\alpha_l\rho_l v_l + \alpha_g\rho_g v_g] + \partial_x\left[\alpha_l\rho_l v_l^2 + \alpha_g\rho_g v_g^2 + p\right] &= -q. \end{aligned} \tag{4}$$

We now describe this model in more detail. First, we assume that there is no mass transfer between the phases, hence

$$\Gamma_l = \Gamma_g = 0.$$

Furthermore, for computational purposes we assume an analytical slip law of the form

$$v_g = K v_{\text{mix}} + S, \tag{5}$$

where $v_{\text{mix}} = \alpha_l v_l + \alpha_g v_g$ is the mixture average velocity and K, S are flow-dependent parameters. We assume that the liquid density has the form

$$\rho_l = \rho_{l,0} + \frac{p - p_{l,0}}{a_l^2}, \tag{6}$$

where $a_l = 1000$ m/s is the velocity of sound in the liquid phase and $\rho_{l,0}$ and $p_{l,0}$ are given constants. Here we will assume that $\rho_{l,0} = 1000\ \text{kg/m}^3$ and $p_{l,0} = 1$ bar. For the gas density, we assume the form

$$\rho_g = \frac{p}{a_g^2}, \tag{7}$$

where $a_g = 316$ m/s is the velocity of sound in the gas phase. The volume fractions are related by

$$\alpha_l + \alpha_g = 1.$$

Finally, for the source term q we have

$$q = F_w + F_g,$$

where $F_g = g(\alpha_l\rho_l + \alpha_g\rho_g)\sin\theta$ represents the gravity where g is the gravitational constant and θ is the inclination. The viscous forces and forces between the wall and the fluids are taken into account through the frictional force term F_w given by the following simple model

$$F_w = \frac{32 v_{\text{mix}}\mu_{\text{mix}}}{d^2}, \tag{8}$$

where d is the inner diameter and the mixed viscosity μ_{mix} is given by

$$\mu_{\text{mix}} = \alpha_l\mu_l + \alpha_g\mu_g,$$

and the viscosity for liquid and gas are assumed to be $\mu_l = 5 \times 10^{-2}$ Pa s and $\mu_g = 5 \times 10^{-6}$ Pa s respectively.

We can write the system (4) in the conservative vector form

$$\partial_t \mathbf{w} + \partial_x F(\mathbf{w}) = G(\mathbf{w}), \tag{9}$$

where

$$\mathbf{w} = \begin{pmatrix} \alpha_l \rho_l \\ \alpha_g \rho_g \\ \alpha_l \rho_l v_l + \alpha_g \rho_g v_g \end{pmatrix}, \qquad F(\mathbf{w}) = \begin{pmatrix} \alpha_l \rho_l v_l \\ \alpha_g \rho_g v_g \\ \alpha_l \rho_l v_l^2 + \alpha_g \rho_g v_g^2 + p \end{pmatrix},$$

$$G(\mathbf{w}) = \begin{pmatrix} 0 \\ 0 \\ -q \end{pmatrix}. \tag{10}$$

It can also be instructive to express the above system in the form

$$\partial_t \begin{pmatrix} w_1 \\ w_2 \\ w_3 \end{pmatrix} + \partial_x \begin{pmatrix} v_l w_1 \\ v_g w_2 \\ v_l^2 w_1 + v_g^2 w_2 + p(w_1, w_2) \end{pmatrix} = \begin{pmatrix} 0 \\ 0 \\ -q \end{pmatrix}, \tag{11}$$

where $w_1 = \alpha_l \rho_l$, $w_2 = \alpha_g \rho_g$, and $w_3 = \alpha_l \rho_l v_l + \alpha_g \rho_g v_g$. Note that pressure $p = p(w_1, w_2)$ is a passive variable obtained from the conservative variables w_1 and w_2. This is used in the numerical algorithms presented later. For a more comprehensive discussion of mathematical properties of the drift-flux model we refer to [20] and [1]. Here we will just recall that under the condition of incompressible liquid and when

$$\alpha_g \rho_g \ll \alpha_l \rho_l, \tag{12}$$

for two-phase regions where $\alpha_g \in (0, 1)$, the following *approximative* sound velocity has been devised:

$$\omega^2 = \frac{p}{\alpha_g \rho_l (1 - K \alpha_g)}. \tag{13}$$

The corresponding eigenvalues are given by

$$\lambda_1 = v_l - \omega, \qquad \lambda_2 = v_g, \qquad \lambda_3 = v_l + \omega. \tag{14}$$

The first and third eigenvalues correspond to pressure pulses propagating downstream and upstream while the second eigenvalue represents the wave speed of the gas volume wave traveling downstream. For pure liquid regions ($\alpha_g = 0$) we have

$$\lambda_1 = v_l - a_l, \qquad \lambda_3 = v_l + a_l, \tag{15}$$

where a_l is the sound velocity of the liquid phase. These eigenvalues correspond to pressure pulses propagating upstream and downstream. Similarly, for pure gas regions ($\alpha_g = 1$) we have

$$\lambda_1 = v_g - a_g, \qquad \lambda_3 = v_g + a_g, \tag{16}$$

where a_g is the sound velocity of the gas phase:

Remark 1. Note that the drift-flux model (4) and the two-fluid model (3) both consist of two mass conservation equations. As far as accurate and robust calculation of contact discontinuities is concerned, one might expect that the two models are closely interrelated. Hence, by investigating numerical schemes for the drift-flux model we also seek insight into the basic mechanisms relevant to developing accurate and robust numerical schemes for the two-fluid model.

Remark 2. The analytical slip law (5) which describes the relation between v_l and v_g can be replaced by more general models. In particular, for more realistic flows the slip velocity between the two phases should be given by a hydrodynamical model that accounts for the different flow regimes. Similarly, the models for fluid properties given by the density models (6) and (7) should be replaced by more general thermodynamical models. However, methods developed in this paper still apply. See Section 7.4 for more on this.

Remark 3. Regarding two-phase flow in pipelines, it is convenient to identify three classes of physical phenomena which all work on different time scales [19]. These are interphase exchanges, fluid transport, and propagation of pressure pulses (sonic waves). This paper focuses on the last two phenomena. Concerning transport of gas and liquid, the high compressibility of the gas phase relative to the liquid phase leads to a highly dynamic process. The flow behavior will depend greatly on the pressure development in the pipeline which in turn is determined by effects related to wall friction and hydrostatic conditions. On the other hand, pressure pulses are mainly caused by inlet flow rate changes. These waves have a characteristic time scale that is 10–100 times smaller than the transient behavior of fluid transport. The pressure waves are usually small in magnitude and propagate as small perturbations of the pressure generated by the dynamics of mass transport.

Remark 4. A notable fact is that the two-phase mixture has a much lower sonic velocity than both pure liquid and gas. If we consider a plot of the sonic velocity as a function of the gas volume fraction, we will see that the acoustic velocity changes very rapidly in the "one-phase to two-phase" transition regions [10, 17]. Typically, the sound speed can be several orders of magnitude higher in the liquid phase than in the two-phase mixture. This gives rise to strong nonlinear effects.

3. FLUX-SPLITTING SCHEMES

Instead of discretizing the flux F of (4) directly, we want to treat the convection and pressure terms separately in the discretization procedure. The natural splitting of the total flux into convective and pressure parts is given by

$$F = F_c + F_p = \begin{pmatrix} \alpha_l \rho_l v_l \\ \alpha_g \rho_g v_g \\ \alpha_l \rho_l v_l^2 + \alpha_g \rho_g v_g^2 \end{pmatrix} + \begin{pmatrix} 0 \\ 0 \\ p \end{pmatrix}. \tag{17}$$

A finer treatment of the convective flux can be taken by considering a further breakup as follows:

$$F_c = F_{c,l} + F_{c,g} = \alpha_l \rho_l v_l \begin{pmatrix} 1 \\ 0 \\ v_l \end{pmatrix} + \alpha_g \rho_g v_g \begin{pmatrix} 0 \\ 1 \\ v_g \end{pmatrix}. \tag{18}$$

Based on this splitting we now describe three different numerical schemes.

3.1. *Two Hybrid FDS/FVS Schemes: AUSM and Van Leer*

It is well known that there is an excessive dissipation at contact discontinuities associated with FVS schemes. This will be demonstrated below for the current two-phase model. On the other hand FDS schemes perform very well for contact discontinuities. This motivates us to try to eliminate the surplus dissipation of the FVS by introducing the flavor of the FDS into FVS schemes. Following [24] we now describe two such approaches. Basically, the idea is to identify a suitable "convective speed" and then implement upwind principles in the discretization of the convective terms. Starting with (17) and (18) we now focus on two different constructions where this idea is carried out. In view of (18) a natural choice for defining the interface convective speed is the mass fluxes $(\alpha_l\rho_l v_l)_{j+1/2}$ and $(\alpha_g\rho_g v_g)_{j+1/2}$, which provide the sign as well as value appropriate for upwinding. The numerical flux at the interface $j+1/2$ can then be written as

$$\begin{aligned} F_{j+1/2}(\mathbf{w}_L,\mathbf{w}_R) = {} & \frac{1}{2}\big[(\alpha_l\rho_l v_l)_{j+1/2}(\mathbf{\Phi}_{l,L}+\mathbf{\Phi}_{l,R}) - \big|(\alpha_l\rho_l v_l)_{j+1/2}\big|(\mathbf{\Phi}_{l,R}-\mathbf{\Phi}_{l,L})\big] \\ & + \frac{1}{2}\big[(\alpha_g\rho_g v_g)_{j+1/2}(\mathbf{\Phi}_{g,L}+\mathbf{\Phi}_{g,R}) - \big|(\alpha_g\rho_g v_g)_{j+1/2}\big| \\ & \times(\mathbf{\Phi}_{g,R}-\mathbf{\Phi}_{g,L})\big] + (F_p)_{j+1/2}, \end{aligned} \tag{19}$$

where $\mathbf{\Phi}_l = (1, 0, v_l)^T$, $\mathbf{\Phi}_g = (0, 1, v_g)^T$, and $F_p = (0, 0, p)^T$. Here the interface mass fluxes $(\alpha_l\rho_l v_l)_{j+1/2}$ and $(\alpha_g\rho_g v_g)_{j+1/2}$ can be chosen in different ways. We follow along the line of Wada and Liou [24], who considered single-phase flow, and propose the following Van Leer and AUSM schemes for two-phase flow (we use the same discretization for both phases).

- Van Leer type:

$$(\alpha\rho v)^{\text{Van Leer}}_{j+1/2} = V^+\big(v_L, c_{j+1/2}\big)\alpha_L\rho_L + V^-\big(v_R, c_{j+1/2}\big)\alpha_R\rho_R. \tag{20}$$

- AUSM type (U-splitting):

$$(\alpha\rho v)^{\text{AUSM}}_{j+1/2} = \frac{1}{2}\big[v_{j+1/2}(\alpha_L\rho_L+\alpha_R\rho_R) - \big|v_{j+1/2}\big|(\alpha_R\rho_R-\alpha_L\rho_L)\big], \tag{21}$$

where $v_{j+1/2} = v_L^+ + v_R^-$ and $v_L^+ = V^+(v_L, c_{j+1/2})$ and $v_R^- = V^-(v_R, c_{j+1/2})$. We observe that since we use a common sound velocity, the AUSM M-splitting and U-splitting coincide. Here the velocity-splitting formulas $V^\pm$ are defined by

$$V^\pm(v,c) = \begin{cases} \pm\frac{1}{4c}(v\pm c)^2 & \text{if } |v|\le c \\ \frac{1}{2}(v\pm|v|) & \text{otherwise.} \end{cases} \tag{22}$$

In particular, the splitting functions $V^\pm$ satisfy the consistency condition

$$V^+(v,c) + V^-(v,c) = v. \tag{23}$$

For the pressure term F_p, an FVS type discretization of the following form is used,

$$p_{j+1/2} = P^+\big(v_L, c_{j+1/2}\big)\,p_L + P^-\big(v_R, c_{j+1/2}\big)\,p_R, \tag{24}$$

where v is a mixed fluid velocity, and the pressure-splitting formulas $P^{\pm}$ are given by

$$P^{\pm}(v, c) = V^{\pm}(v, c) \cdot \begin{cases} \frac{1}{c}\left(\pm 2 - \frac{v}{c}\right) & \text{if } |v| \leq c \\ \frac{1}{v} & \text{otherwise.} \end{cases} \tag{25}$$

For the definition of a sound velocity c associated with the mixture, we obtain an approximate sound velocity using the model

$$c(\alpha_g) = \begin{cases} a_l & \text{if } \alpha_g < \varepsilon \\ \omega & \text{if } \varepsilon \leq \alpha_g \leq 1 - \varepsilon \\ a_g & \text{if } \alpha_g > 1 - \varepsilon, \end{cases} \tag{26}$$

where ω is given by (13) and ε is a small parameter whose purpose is to ensure that we have a smooth transition from a two-phase to a single-phase sound velocity. We have used $\varepsilon = 0.001$ for all simulations presented in this work. We define a common speed $c_{j+1/2}$ associated with the interface $j + 1/2$ which is an average of c_L and c_R. Note that a common sound speed has been used before for Euler equations for both AUSMDV [24] and AUSM+ [14]. Following [24] we will use the choice $c = \max(c_L, c_R)$ in this work. For the discretization of the pressure term occurring in the mixed momentum equation we need a fluid velocity for the mixture of the two phases. One natural choice is to consider a mixed fluid velocity v_{mix} given by

$$v = v_{\text{mix}} = \alpha_l v_l + \alpha_g v_g. \tag{27}$$

This choice is motivated by the fact that for the flow cases we study in this work, it is reasonable to assume that both phasic mass fluxes behave as if they are subsonic. The above definition of v_{mix} ensures that the pressure term will be treated as subsonic as well. More generally, one should also explore other choices which guarantee a consistent discretization of the convective and pressure terms.

3.2. *An FVS Scheme*

We now briefly describe an FVS scheme for our two-phase model. The discretization of the pressure term remains the same; for the convective terms, we use the discretization

$$\begin{aligned} F^{\text{FVS}}_{j+1/2}(\mathbf{w}_L, \mathbf{w}_R) = {} & (\alpha_l \rho_l)_L \boldsymbol{\Psi}^+_{l,L} + (\alpha_l \rho_l)_R \boldsymbol{\Psi}^-_{l,R} + (\alpha_g \rho_g)_L \boldsymbol{\Psi}^+_{g,L} \\ & + (\alpha_g \rho_g)_R \boldsymbol{\Psi}^-_{g,R} + (F_p)_{j+1/2}, \end{aligned} \tag{28}$$

where $F_p = (0, 0, p)^T$ and

$$\boldsymbol{\Psi}^+_{l,L} = \boldsymbol{\Psi}^+_l\left(v_{l,L}, c_{j+1/2}\right), \qquad \boldsymbol{\Psi}^-_{l,R} = \boldsymbol{\Psi}^-_l\left(v_{l,R}, c_{j+1/2}\right), \tag{29}$$

where

$$\boldsymbol{\Psi}^+_l(v, c) = V^+(v, c) \begin{pmatrix} 1 \\ 0 \\ v \end{pmatrix}, \qquad \boldsymbol{\Psi}^-_l(v, c) = V^-(v, c) \begin{pmatrix} 1 \\ 0 \\ v \end{pmatrix}, \tag{30}$$

where the velocity-splitting formulas $V^{\pm}$ are given by (22). Similarly, we have for the gas phase

$$\Psi_g^+(v,c) = V^+(v,c)\begin{pmatrix}0\\1\\v\end{pmatrix}, \qquad \Psi_g^-(v,c) = V^-(v,c)\begin{pmatrix}0\\1\\v\end{pmatrix}, \tag{31}$$

and

$$\mathbf{\Psi}_{g,L}^+ = \mathbf{\Psi}_g^+\big(v_{g,L}, c_{j+1/2}\big), \qquad \mathbf{\Psi}_{g,R}^- = \mathbf{\Psi}_g^-\big(v_{g,R}, c_{j+1/2}\big). \tag{32}$$

Note that this FVS scheme coincides with the Van Leer scheme for the mass conservation equations, while the discretization of the mixed momentum equation is different. Finally, we note that our scheme is really an FVS scheme since we can write the flux in the form

$$F_{j+1/2}^{\mathrm{FVS}}(\mathbf{w},\mathbf{w}) = F^-(\mathbf{w}) + F^+(\mathbf{w}), \tag{33}$$

where

$$F^-(\mathbf{w}) = \alpha_l\rho_l\mathbf{\Psi}_l^+(v_l,c) + \alpha_g\rho_g\mathbf{\Psi}_g^+(v_g,c) + \begin{pmatrix}0\\0\\P^+(v_{\mathrm{mix}},c)\end{pmatrix}p$$

$$F^+(\mathbf{w}) = \alpha_l\rho_l\mathbf{\Psi}_l^-(v_l,c) + \alpha_g\rho_g\mathbf{\Psi}_g^-(v_g,c) + \begin{pmatrix}0\\0\\P^-(v_{\mathrm{mix}},c)\end{pmatrix}p.$$

Due to the relations

$$\mathbf{\Psi}_l^+(v,c) + \mathbf{\Psi}_l^-(v,c) = \begin{pmatrix}v\\0\\v^2\end{pmatrix}, \qquad \mathbf{\Psi}_g^+(v,c) + \mathbf{\Psi}_g^-(v,c) = \begin{pmatrix}0\\v\\v^2\end{pmatrix},$$

$$P^+(v,c) + P^-(v,c) = 1,$$

we can conclude that (33) holds. In the following sections we will investigate some basic properties possessed by the three schemes introduced above.

3.3. *Extension to Second-Order Spatial and Temporal Accuracy*

A second-order variant of the various schemes for the two-phase model is obtained by using the classical MUSCL technique [23]. We choose to extrapolate the primitive variables $\mathbf{u} = (\alpha_l, \alpha_g, \rho_l, \rho_g, v_l, v_g)$ (rather than the conservative variables $\mathbf{w}$). This is done according to the formulas

$$\mathbf{u}_L := \mathbf{u}_j + \frac{\Delta x}{2}S(D_-\mathbf{u}_j, D_+\mathbf{u}_j), \qquad \mathbf{u}_R := \mathbf{u}_{j+1} - \frac{\Delta x}{2}S(D_-\mathbf{u}_{j+1}, D_+\mathbf{u}_{j+1}), \tag{34}$$

where $S(u,v)$ is the slope limiter. We have used the Van Leer limiter in the numerical experiments. Second-order accuracy in time is obtained by using a two-stage Runge–Kutta discretization.

3.4. *Boundary Treatment*

Because of the hyperbolic nature of the model we are studying, it is important to treat precisely the information going in and out of the system. The treatment of the boundary conditions takes into account the information going out of the system through a set of compatibility conditions. These are solved together with the imposed boundary conditions using an upwind discretization. Considering the last two test cases studied in this work, we specify some mass flow rates at the inlet of the pipeline, while keeping the pressure constant at the outlet end. For more details we refer to [11].

4. SOME NUMERICAL EXAMPLES

The purpose of the numerical experiments is to reveal differences and similarities among the three schemes developed above. In particular, we want to explore the ability of the various schemes to produce monotone and accurate discontinuity profiles in pressure, fluid velocities, and volume fraction. First, we consider a two-phase shock tube problem. Then, we consider a flow case characterized by fast transients (propagation of sonic waves). In the third example, we consider the slower transient of liquid and gas transport. In particular, we wish to treat the most difficult case where one of the phases disappears. See also Remark 3 for more on various flow phenomena.

Since the discrete fluxes are treated explicitly in time, the schemes presented above are subject to the (CFL) condition

$$\Delta t = \mathrm{CFL}\frac{\Delta x}{\max(|\lambda_1|, |\lambda_2|, |\lambda_3|)}, \tag{35}$$

where λ_i is given by (14), (15), and (16). For the first example we use the rough estimate $\max(|\lambda_1|, |\lambda_2|, |\lambda_3|) \approx 30$, while for the last two we apply the estimate $\max(|\lambda_1|, |\lambda_2|, |\lambda_3|) \approx 1000$. We also note that in the numerical algorithms, pressure is obtained as a passive variable from the conservative variables w_1, w_2. Generally, it is not possible to calculate any analytical solution for the two-phase model. Consequently, for the various flow cases presented, we have computed a reference solution by using the AUSMV scheme described in Section 6 on a fine grid.

4.1. *Shock Tube Problem*

Following [1, 11] we consider a slightly simplified model by assuming that the liquid density is constant $\rho_l = 1000$ kg/m^3 and by neglecting the wall friction F_w. Furthermore, we use the slip law (5) where $K = 1.07$ and $S = 0.216$. A horizontal pipe of length 100 m is considered, which initially is separated in a left and right state at $x_0 = 50$ m. More precisely, we assume the initial data

$$\begin{aligned} \alpha_{g,L} &= 0.55, \quad & v_{l,L} &= 10.370 \text{ m/s}, \quad & p_L &= 80450 \text{ Pa} \\ \alpha_{g,R} &= 0.55, \quad & v_{l,R} &= 0.561 \text{ m/s}, \quad & p_R &= 24282 \text{ Pa}. \end{aligned}$$

For the numerical calculations we use CFL $= 1.0$ together with a space discretization $\Delta x = 0.5$ m. Simulation results for FVS, Van Leer, and AUSM are presented in Figs. 1–3. We have plotted the gas volume fraction, liquid velocity, and pressure at time $t = 1.0$ s.

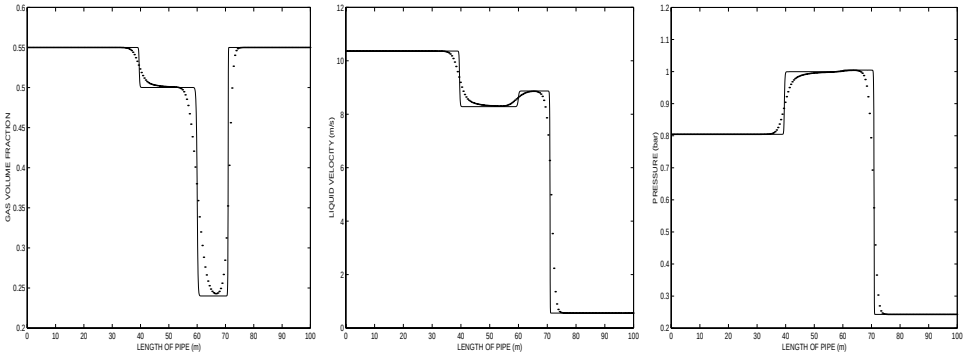

FIG. 1. First-order FVS. Left: Gas volume fraction. Middle: Liquid velocity. Right: Pressure. The plots are considered after $t = 1.0$ s.

The solution of this problem is composed of a 1-shock, a 2-contact, and a 3-shock. Since our main interest is characteristic properties related to stability and accuracy of the various schemes we have only computed first-order approximations.

We observe that the results obtained with all three schemes are in good agreement. We may conclude that this flow problem reveals no essential difference among the three schemes.

4.2. *Fast Transients—Propagation of Pressure Pulses*

Next, we focus on an example with fast transients where fast-moving sonic (acoustic) waves in pressure and fluid velocities occur. A similar test case was used in [11]. For our test case we assume that we have a 1000-m-long pipe with diameter 10 cm. The first 750 m are filled with 99% liquid and 1% gas while the last 250 m are filled with 10% liquid and 90% gas. The pressure is initially 1 bar in the pipeline and the fluids are stagnant. For simplicity we have considered the no-slip case $v_l = v_g$. We now introduce a pulse in pressure and fluid velocities by increasing the inlet liquid rate from 0 to 0.3 kg/s in 0.0025 s. We use CFL $= 1.0$ and a space discretization $\Delta x = 10$ m. The first-order simulation results for FVS, Van-Leer, and AUSM are shown in Figs. 4–6. Discontinuity waves are formed in pressure and velocity which move with a sound velocity of approximately 100 m/s before they reach

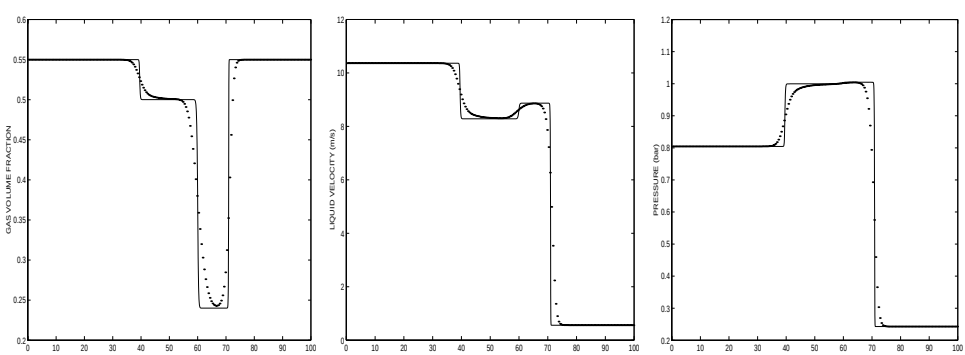

FIG. 2. First-order Van Leer. Left: Gas volume fraction. Middle: Liquid velocity. Right: Pressure. The plots are considered after $t = 1.0$ s.

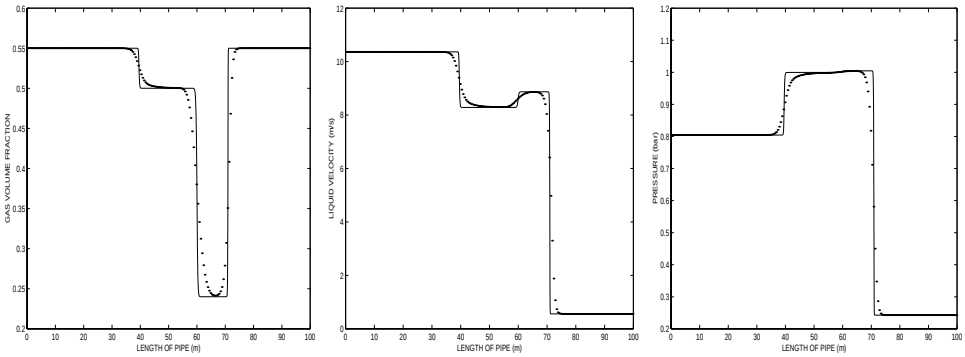

FIG. 3. First-order AUSM. Left: Gas volume fraction. Middle: Liquid velocity. Right: Pressure. The plots are considered after $t = 1.0$ s.

the gas-dominated region, where the sound velocity becomes approximately 30 m/s. When these pulses experience the sudden change in the gas volume fraction located at 750 m the changes in compressibility and sound velocity produce reflecting waves in pressure and velocity, (see also Remark 4).

4.2.1. FVS and Van Leer. From Fig. 4 we observe that FVS has a very good ability to produce nonoscillatory approximations of the acoustic waves in pressure and fluid velocity. However, the approximation of the stationary gas volume fraction contact discontinuity is poor (left plot). For that reason a strong loss of accuracy is seen in pressure and velocity after the pulses have reached the gas-dominated region starting at 750 m. Discontinuities in pressure and velocity are misplaced (see middle and right plots) as well as smeared out because of the strong smearing of the gas volume contact discontinuity. Figure 5 shows that the solution produced by the Van Leer scheme is close to the FVS scheme. However, we see that the Van Leer scheme introduced a slight oscillation in pressure and velocity after time $t = 2.5$ s (see middle and right plots).

4.2.2. AUSM. The AUSM scheme has vanishing numerical dissipation at the stationary gas volume fraction contact discontinuity. This is clearly demonstrated in Fig. 6 (left plot). However, AUSM produces a highly oscillatory approximation of the pressure and velocity waves, which makes it unsuitable for accurate calculations of fast transients such as those introduced in the current flow case.

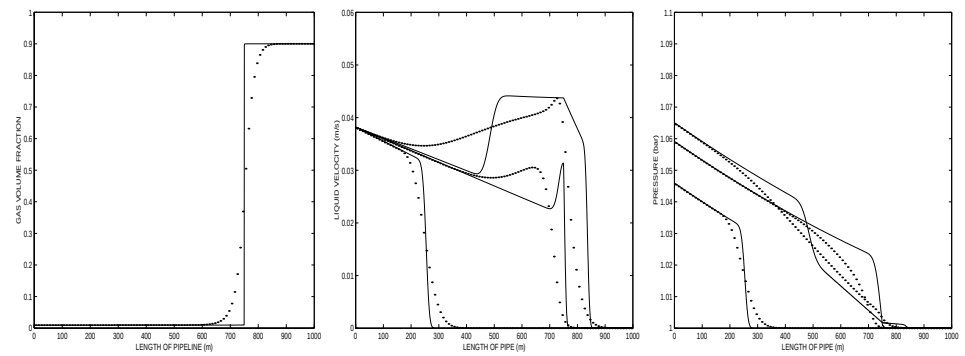

FIG. 4. First-order FVS. Left: Gas volume fraction after $t = 7.5$ s. Middle: Liquid velocity. Right: Pressure. The plots of liquid velocity and pressure are considered after $t = 2.5$, 7.5, and 10.0 s.

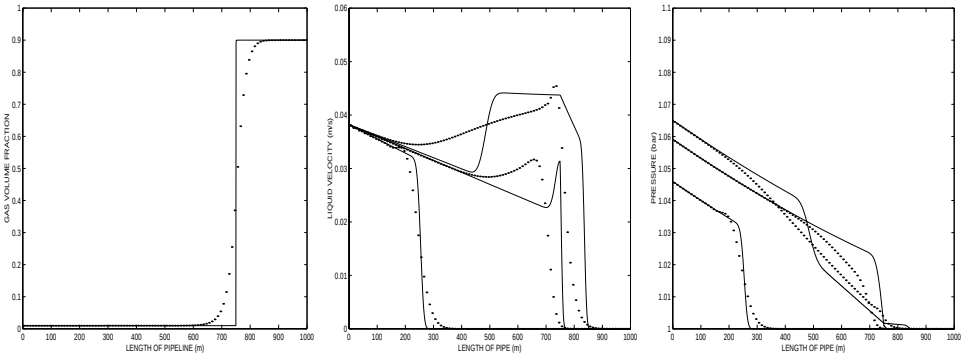

FIG. 5. First-order Van Leer. Left: Gas volume fraction after $t = 7.5$ s. Middle: Liquid velocity. Right: Pressure. The plots of liquid velocity and pressure are considered after $t = 2.5$, 7.5, and 10.0 s.

4.2.3. Some remarks. Accurate and robust simulation of propagation of pulses in pressure and fluid velocities is indeed a challenging task since it typically involves both discontinuities where the gas–liquid mixture stays in a mechanical nonequilibrium state and volume fraction contact discontinuities where the gas–liquid mixture stays in an equilibrium state. It seems that of the three schemes, the FVS scheme has the best ability to capture strong discontinuities. However, the dissipative mechanism of FVS is a "disaster" for stationary volume fraction contact discontinuities. To demonstrate that this is a fundamental problem, we calculated the solution by using a second-order variant of FVS where we used the Van Leer slope limiter, see Fig. 7. Due to the smearing of the volume fraction contact discontinuity, the propagating waves are still misplaced and a sharp "spike" is produced in the fluid velocity after time $t = 10$ s. On the other hand, the dissipation provided in AUSM does not seem, to be sufficient to deal with the mechanical nonequilibrium state discontinuity of this test case; however, it handles stationary contact discontinuities without introducing numerical diffusion.

4.3. *Slow Transients—Transport of a Gas Volume Fraction Contact Discontinuity*

Now we want to check the FVS, Van-Leer and AUSM schemes and their performance on the transport of a slowly moving linear gas volume fraction wave (moving contact

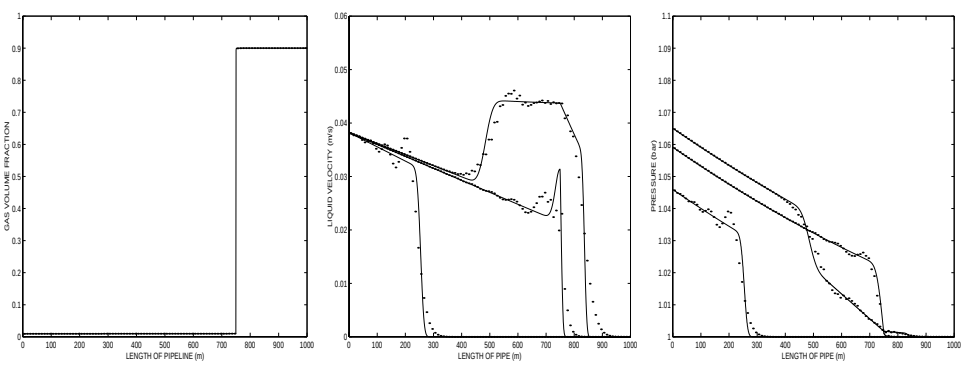

FIG. 6. First-order AUSM. Left: Gas volume fraction after $t = 7.5$ s. Middle: Liquid velocity. Right: Pressure. The plots of liquid velocity and pressure are considered after $t = 2.5$, 7.5, and 10.0 s.

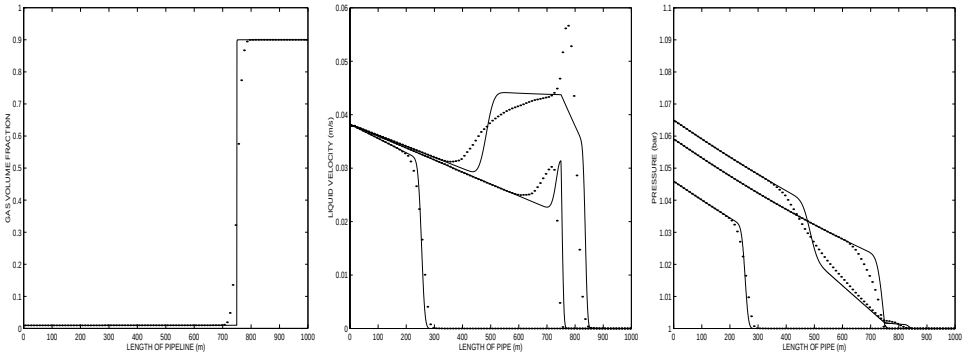

FIG. 7. Second-order FVS. Left: Gas volume fraction after $t = 7.5$ s. Middle: Liquid velocity. Right: Pressure. The plots of liquid velocity and pressure are considered after $t = 2.5$, 7.5, and 10.0 s.

discontinuity). A good approximation of volume fraction contact discontinuities is a fundamental and critical point for many interesting mass transport problems described by our model. Of particular interest are those contact discontinuities which separate a two-phase region from a single-phase region. A crucial point is that the scheme should handle well the transition from single-phase flow to two-phase flow without introducing oscillations in the neighborhood of the discontinuity because such oscillations would typically lead to negative masses.

We consider transport of a gas volume fraction contact discontinuity from left to right obtained by injecting a mixture of gas and liquid at the (left) inlet end. More precisely, initially the pipe is filled with stagnant liquid. The gas and liquid mass flow rates are increased to 0.02 kg/s and 3.0 kg/s, respectively, in 10 s. At the outlet boundary, the pressure is kept constant at 1 bar. For all schemes we use a CFL number of 1.2, and space discretization $\Delta x = 20$ m. The simulation results produced by the first-order schemes for FVS, Van Leer, and AUSM are shown in Figs. 8–10, while the performance of the corresponding second-order schemes are shown in Figs. 11–13. For the second-order schemes we used the Van Leer limiter to extrapolate the primitive variables, except for the pressure variable, for which we used only a first-order treatment. The extrapolation of the pressure variable tended to introduce some slight oscillations in the liquid velocity.

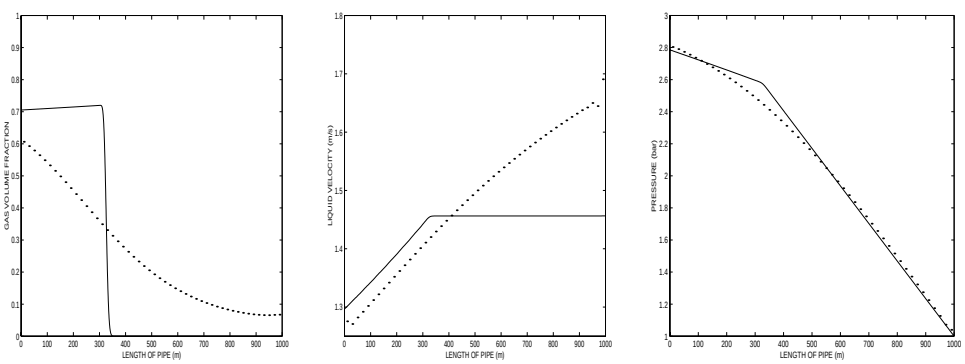

FIG. 8. First-order FVS. Left: Gas volume fraction. Middle: Liquid velocity. Right: Pressure. The plots are considered after $t = 250$ s.

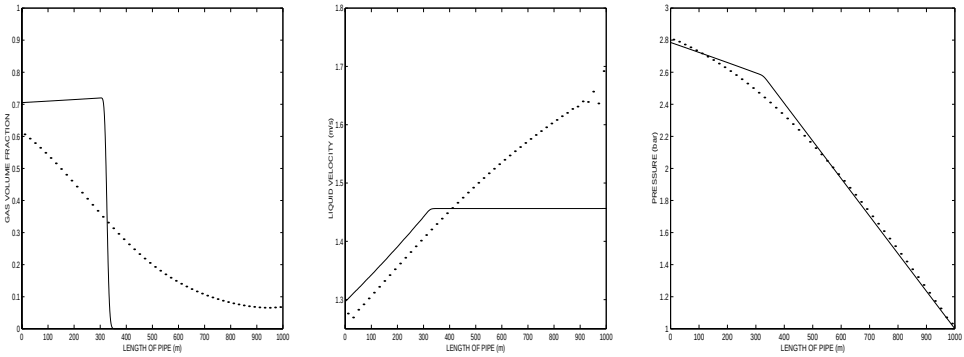

FIG. 9. First-order Van Leer. Left: Gas volume fraction. Middle: Liquid velocity. Right: Pressure. The plots are considered after $t = 250$ s.

4.3.1. FVS and Van Leer. The first-order schemes of FVS and Van Leer give results that are very similar (Figs. 8 and 9). Most notably, both of them introduced an excessive smearing of the moving gas volume fraction contact discontinuity, which makes them unsuitable for typical mass transport simulation problems. In addition, both schemes tended to produce some oscillations in the liquid velocity close to the outlet; see the middle plots of Figs. 8 and 9. The results produced by the second-order variants of the FVS and Van Leer schemes are shown in Figs. 11 and 12. We observe that these results are much better than the first-order approximation. However, the gas front is still smeared out to a large extent. The numerical dissipation seems to be especially strong in the pure liquid region on the right side of the front. In fact, from Figs. 11 and 12 (left plots) we see that there is some gas present throughout the whole pipeline which produces inaccuracy in the approximation of the fluid velocity as well (middle plots).

4.3.2. AUSM. From Fig. 10 we see that the first-order AUSM scheme performs very well for this flow case. Also Fig. 13 demonstrates that the second-order AUSM scheme yields an accurate and nonoscillatory resolution of the gas volume fraction contact discontinuity as well as excellent approximations of fluid velocity and pressure with no tendency to oscillation are observed. Thus this scheme seems to be very suitable for flow cases where the dynamics of mass transport is the main interest.

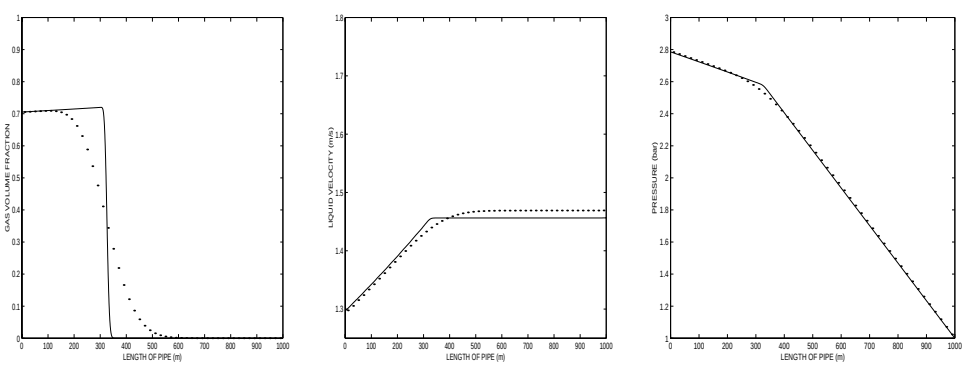

FIG. 10. First-order AUSM. Left: Gas volume fraction. Middle: Liquid velocity. Right: Pressure. The plots are considered after $t = 250$ s.

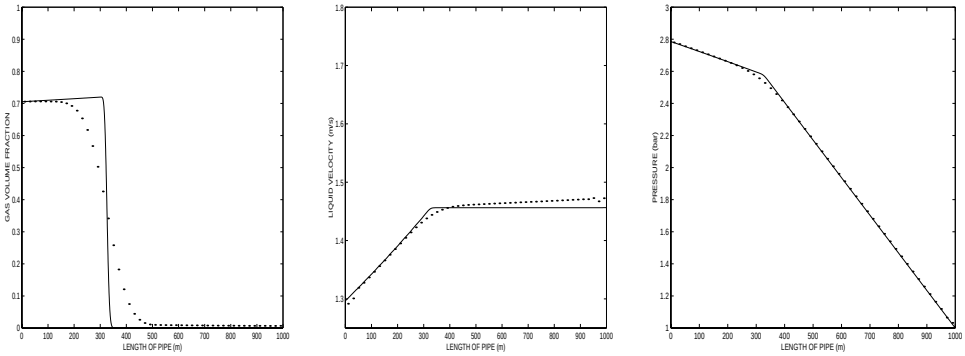

FIG. 11. Second-order FVS. Left: Gas volume fraction. Middle: Liquid velocity. Right: Pressure. The plots are considered after $t = 250$ s.

4.3.3. Some remarks. The two-phase AUSM scheme presented in this paper seems to be a well-designed hybrid FVS/FDS scheme for simulation of mass flow dynamic (slow transients) described by the current two-phase model. However, as observed in the second test case, the AUSM scheme does not combine FVS and FDS in a way that enables it to approximate well both propagation of sonic waves and stationary or moving contact discontinuities. This motivates us to try to design hybrid schemes that combine in a suitable way the best properties from the FVS and AUSM schemes. A first step in that direction is to locate the dissipative mechanisms of the various schemes. This is the purpose of the next section.

5. ANALYSIS OF THE NUMERICAL DISSIPATION MECHANISM

Two main observations were made from the numerical experiments of the previous section:

- The AUSM scheme treats steady and moving contact discontinuities accurately.
- The FVS scheme is able to capture acoustic waves in a monotone and accurate way.

Now, we seek to obtain analytical expressions for the numerical fluxes corresponding to the various schemes. In particular, we want to identify what is a "good" numerical flux for the accurate and robust approximation of contact discontinuities that are steady as well as moving.

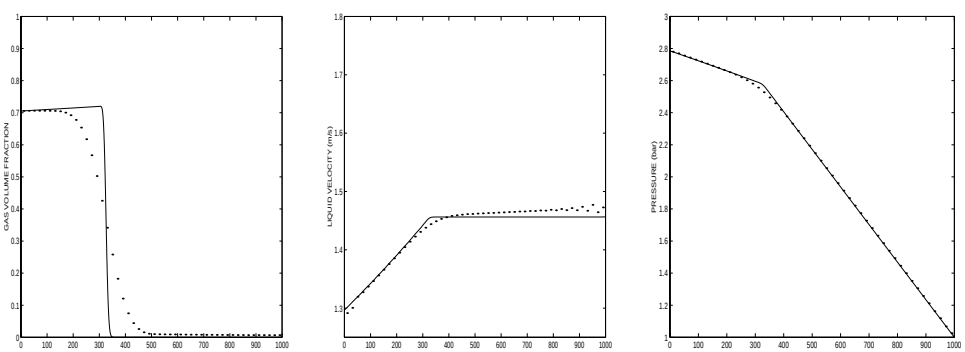

FIG. 12. Second-order Van Leer. Left: Gas volume fraction. Middle: Liquid velocity. Right: Pressure. The plots are considered after $t = 250$ s.

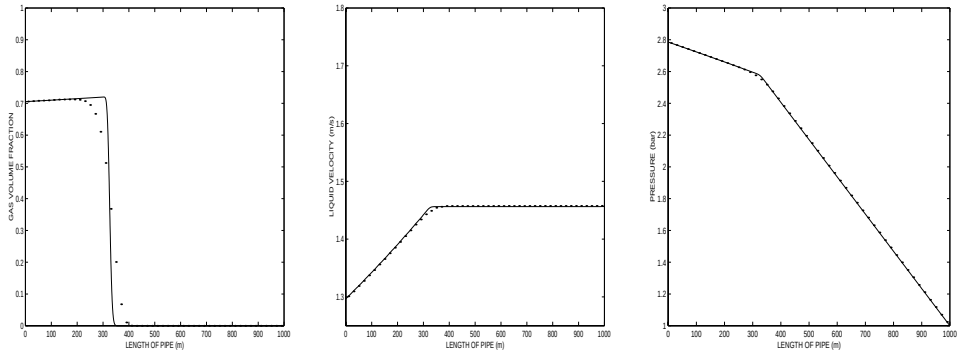

FIG. 13. Second-order AUSM. Left: Gas volume fraction. Middle: Liquid velocity. Right: Pressure. The plots are considered after $t = 250$ s.

5.1. *Dissipative Mechanism of the Three Schemes*

From (21) it follows directly that the AUSM mass flux can be written in the viscous form

$$\begin{aligned}(\alpha_k\rho_k v_k)^{\text{AUSM}}_{j+1/2} &= v_{k,j+1/2}\frac{(\alpha_k\rho_k)_L + (\alpha_k\rho_k)_R}{2} - \frac{1}{2}d^{\text{AUSM}}_{k,j+1/2}\\ d^{\text{AUSM}}_{k,j+1/2} &= \left|v_{k,j+1/2}\right|((\alpha_k\rho_k)_R - (\alpha_k\rho_k)_L) \qquad k = l, g,\end{aligned} \tag{36}$$

where $v_{k,j+1/2} = V^+(v_{k,L}, c_{j+1/2}) + V^-(v_{k,R}, c_{j+1/2})$. By comparing (19) and the definition of $\mathbf{\Phi}$ with (28) and the definition of $\mathbf{\Psi}$, we see that the mass flux of FVS and Van Leer coincide. In particular, the FVS (and Van Leer) mass flux can be expressed as

$$\begin{aligned}(\alpha_k\rho_k v_k)^{\text{FVS}}_{j+1/2} &= \frac{(v_k\alpha_k\rho_k)_L + (v_k\alpha_k\rho_k)_R}{2} - \frac{1}{2}d^{\text{FVS}}_{k,j+1/2}\\ d^{\text{FVS}}_{k,j+1/2} &= |V|\big(v_{k,R}, c_{j+1/2}\big)(\alpha_k\rho_k)_R - |V|\big(v_{k,L}, c_{j+1/2}\big)(\alpha_k\rho_k)_L \qquad k = l, g,\end{aligned} \tag{37}$$

where $|V|(v, c) = V^+(v, c) - V^-(v, c)$. This follows from the following arguments. The mass flux of FVS (and Van Leer) is given by

$$(\alpha_k\rho_k v_k)_{j+1/2} = (a_k)_L V^+_{k,L} + (a_k)_R V^-_{k,R} \qquad k = l, g, \tag{38}$$

where $a = \alpha\rho$ and

$$V^+_{k,L} = V^+\big(v_{k,L}, c_{j+1/2}\big), \qquad V^-_{k,R} = V^-\big(v_{k,R}, c_{j+1/2}\big).$$

Now, we make use of the relation (23) and rewrite (38) as

$$(\alpha_k\rho_k v_k)_{j+1/2} = (a_k)_L(v_{k,L} - V^-_{k,L}) + (a_k)_R(v_{k,R} - V^+_{k,R}). \tag{39}$$

Adding expressions (38) and (39) for $(\alpha_k\rho_k v_k)_{j+1/2}$ yields

$$(\alpha_k\rho_k v_k)_{j+1/2} = \frac{(a_k v_k)_L + (a_k v_k)_R}{2} - \frac{1}{2}([V^+_{k,R} - V^-_{k,R}](a_k)_R - [V^+_{k,L} - V^-_{k,L}](a_k)_L),$$

and (37) follows.

5.2. *Numerical Dissipation at Steady and Moving Contact Discontinuities*

First, we assume that we have a moving gas volume contact discontinuity where

$$p_L = p_R = p, \qquad v_{g,L} = v_{g,R} = v_g, \qquad v_{l,L} = v_{l,R} = v_l, \qquad \alpha_{g,L} \neq \alpha_{g,R}. \tag{40}$$

Hence, it follows from (36) that the mass flux of the AUSM scheme becomes ($k = l, g$)

$$(\alpha_k \rho_k v_k)^{\text{AUSM}}_{j+1/2} = v_k \rho_k \frac{\alpha_{k,L} + \alpha_{k,R}}{2} - |v_k| \rho_k \frac{\alpha_{k,R} - \alpha_{k,L}}{2} = \begin{cases} v_k \rho_k \alpha_{k,L} & \text{if } v_k > 0 \\ v_k \rho_k \alpha_{k,R} & \text{otherwise,} \end{cases} \tag{41}$$

where we have used

$$v_{k,j+1/2} = V^+\big(v_k, c_{j+1/2}\big) + V^-\big(v_k, c_{j+1/2}\big) = v_k$$

due to the property (23). In particular, for a steady contact discontinuity where $v_k = 0$ we see that the AUSM scheme has vanishing numerical dissipation, i.e.,

$$(\alpha_k \rho_k v_k)^{\text{AUSM}}_{j+1/2} = 0. \tag{42}$$

Next, let us consider the FVS (Van Leer) scheme. First, we observe that

$$|V|(v, c) = \begin{cases} |v| & |v| > c \\ \frac{1}{2}\left[\frac{v^2}{c} + c\right] & \text{otherwise.} \end{cases} \tag{43}$$

Hence, from (37) and (40) it follows that the mass flux of the FVS (Van Leer) scheme for $|v_k| \leq c$ becomes

$$(\alpha_k \rho_k v_k)^{\text{FVS}}_{j+1/2} = v_k \rho_k \frac{\alpha_{k,L} + \alpha_{k,R}}{2} - \frac{1}{2}\left(\frac{v_k^2}{c_{j+1/2}} + c_{j+1/2}\right) \rho_k \frac{\alpha_{k,R} - \alpha_{k,L}}{2}, \tag{44}$$

for $k = l, g$. In particular, for a stationary contact discontinuity the FVS mass flux assigns a numerical dissipation given by

$$(\alpha_k \rho_k v_k)^{\text{FVS}}_{j+1/2} = -c_{j+1/2} \rho_k \frac{\alpha_{k,R} - \alpha_{k,L}}{4} \neq 0. \tag{45}$$

In view of the analytical expressions for the dissipation mechanism of the various schemes given above, we can explain the results of the numerical experiments in Section 4 as follows:

- AUSM has vanishing dissipation for a stationary gas volume fraction contact discontinuity while FVS and Van Leer introduce a numerical dissipation given by (45). In particular, this numerical dissipation depends on the sound velocity of the two-phase mixture. The difference between these two mass fluxes was clearly observed in the numerical example of Section 4.2 (see left plots of Figs. 4–6).
- In the example presented in Section 4.3, the FVS and Van Leer schemes gave an excessive numerical dissipation for a moving gas volume fraction contact discontinuity. The smearing out effect was especially strong on the side of the gas front adjacent to the pure liquid region; see left plots of Figs. 8–9 and Figs. 11–12. The explanation of this

phenomenon lies in the viscous term of (44) whose value depends directly on the sound velocity $c_{j+1/2}$, which is much higher in the pure liquid region ($c_{j+1/2} = 1000$ m/s) than in the two-phase region (typically $c_{j+1/2} < 50$ m/s). On the other hand, (41) shows that the viscous term of the AUSM flux depends on the fluid velocity for a moving gas volume fraction contact discontinuity.

- The shock tube example of Section 4.1 revealed no essential difference among the various schemes. In particular, the approximation of the gas volume fraction contact discontinuity (the middle discontinuity shown in the left plots of Figs. 1–3) exhibits similar behavior, with the AUSM approximation being slightly sharper. This is because the sound velocity for the two-phase mixture for this example is less than 30 m/s throughout the whole pipeline, while the liquid velocity is about 8 m/s. Consequently, the dissipation terms of the mass fluxes corresponding to the AUSM and FVS (and Van Leer) schemes are not very different in strength.

6. REMOVAL OF NUMERICAL DISSIPATION AT CONTACT DISCONTINUITIES

As observed above, a main drawback of FVS and Van Leer is the excessive numerical dissipation at volume fraction contact discontinuities. Now we seek to eliminate this dissipation following ideas described in [24] for Euler equations.

6.1. *AUSMD and AUSMV*

Using an idea similar to the one applied by Wada and Liou [24] for Euler equations we suggest replacing the velocity-splitting functions $V^{\pm}$ by a more general pair $\tilde{V}^{\pm}$. More precisely, for $|v| \le c$ we define $\tilde{V}^{\pm}$ as a convex combination of $V^{\pm}$ and $(v \pm |v|)/2$, that is

$$\tilde{V}^{\pm}(v, c, \chi) = \begin{cases} \chi V^{\pm}(v, c) + (1-\chi)\frac{v \pm |v|}{2} & |v| \le c \\ \frac{1}{2}(v \pm |v|) & \text{otherwise.} \end{cases} \tag{46}$$

An important feature of the pair $\tilde{V}^{\pm}$ is that it still satisfies the property (23), i.e.,

$$\tilde{V}^{+}(v, c, \chi) + \tilde{V}^{-}(v, c, \chi) = v \qquad \forall (c, \chi). \tag{47}$$

Now we define two new schemes denoted as AUSMV and AUSMD by replacing $V^{\pm}$ by $\tilde{V}^{\pm}$ in the definition of the convective flux part of the FVS and Van Leer scheme respectively. The pressure term F_p is treated as before. In fact, the parameter χ defines a whole family of AUSMV and AUSMD schemes and in the following we will specify how χ can be chosen to obtain "good" numerical fluxes with respect to the accurate approximation of steady and moving contact discontinuities.

First, we observe that the mass flux of AUSMV (and AUSMD) now is given by

$$(\alpha\rho v)_{j+1/2} = (\alpha\rho)_L \tilde{V}_L^{+} + (\alpha\rho)_R \tilde{V}_R^{-}, \tag{48}$$

where

$$\tilde{V}_L^{+} = \tilde{V}^{+}\big(v_L, c_{j+1/2}, \chi_L\big), \qquad \tilde{V}_R^{-} = \tilde{V}^{-}\big(v_R, c_{j+1/2}, \chi_R\big). \tag{49}$$

For simplicity, we have omitted the subscript k denoting the two phases. Since the property (47) still holds, we can show by the same arguments as above that the numerical mass flux of AUSMV (and AUSMD) is given by (37) where the viscous term $d^{\text{FVS}}_{j+1/2}$ now is replaced by

$$d^{\text{AUSMV}}_{j+1/2} = |\tilde{V}|\big(v_R, c_{j+1/2}, \chi_R\big)(\alpha\rho)_R - |\tilde{V}|\big(v_L, c_{j+1/2}, \chi_L\big)(\alpha\rho)_L, \tag{50}$$

where

$$|\tilde{V}|(v, c, \chi) = \tilde{V}^+(v, c, \chi) - \tilde{V}^-(v, c, \chi) = \chi|V|(v, c) + (1-\chi)|v|, \tag{51}$$

where $|V|(v, c) = V^+(v, c) - V^-(v, c)$ as before. In particular, we observe that $|\tilde{V}|$ consists of two terms. In the following, we will see that the purpose of the first one is to enable us to choose χ such that vanishing dissipation is obtained for a steady gas volume fraction contact discontinuity. Moreover, the second term ensures that the AUSM mass flux (41) is recovered for a moving gas volume fraction contact discontinuity.

Thus, the purpose now is to specify the parameters χ_L, χ_R in (50) such that the mass flux of the FVS (and Van Leer) scheme takes the same form as the mass flux of AUSM at a stationary and moving gas volume fraction contact discontinuity.

6.1.1. Stationary contact discontinuity. For a stationary volume fraction contact discontinuity (40) where $v = 0$, we see that (50) becomes

$$\begin{aligned} d^{\text{AUSMV}}_{j+1/2} &= |\tilde{V}|\big(0, c_{j+1/2}, \chi_R\big)(\alpha\rho)_R - |\tilde{V}|\big(0, c_{j+1/2}, \chi_L\big)(\alpha\rho)_L \\ &= \chi_R|V|\big(0, c_{j+1/2}\big)(\alpha\rho)_R - \chi_L|V|\big(0, c_{j+1/2}\big)(\alpha\rho)_L \\ &= |V|\big(0, c_{j+1/2}\big)\rho(p)[\chi_R\alpha_R - \chi_L\alpha_L]. \end{aligned} \tag{52}$$

Consequently, by choosing χ_L, χ_R such that

$$\chi_R\alpha_R - \chi_L\alpha_L = 0 \tag{53}$$

for both phases, no numerical dissipation is introduced in the mass fluxes at the steady contact discontinuity.

6.1.2. Moving contact discontinuity. For a moving volume fraction contact discontinuity (40) with $v \neq 0$ we see that (50) becomes

$$\begin{aligned} d^{\text{AUSMV}}_{j+1/2} &= |\tilde{V}|\big(v, c_{j+1/2}, \chi_R\big)(\alpha\rho)_R - |\tilde{V}|\big(v, c_{j+1/2}, \chi_L\big)(\alpha\rho)_L \\ &= (\chi_R|V|\big(v, c_{j+1/2}\big) + (1-\chi_R)|v|)(\alpha\rho)_R - \big(\chi_L|V|(v, c_{j+1/2}\big) \\ &\quad + (1-\chi_L)|v|)(\alpha\rho)_L \\ &= |v|\rho(p)[\alpha_R - \alpha_L], \end{aligned} \tag{54}$$

where we have used (53). Consequently, in view of (37), (50), and (54) the mass flux becomes

$$(\alpha\rho v)^{\text{AUSMV}}_{j+1/2} = v\rho(p)\frac{\alpha_L + \alpha_R}{2} - \frac{1}{2}|v|\rho(p)[\alpha_R - \alpha_L]. \tag{55}$$

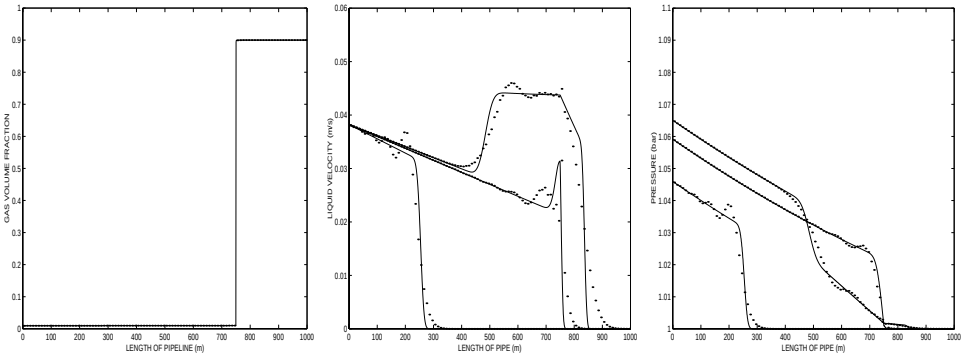

FIG. 14. First-order AUSMD. Left: Gas volume fraction after $t = 7.5$ s. Middle: Liquid velocity. Right: Pressure. The plots of liquid velocity and pressure are considered after $t = 2.5$, 7.5, and 10.0 s.

In other words, the AUSM mass flux (41) is recovered. Many different choices can be made for χ_L, χ_R such that (53) is satisfied. Here we simply use

$$\chi_L = \alpha_R, \qquad \chi_R = \alpha_L. \tag{56}$$

Hence, in the following, AUSMV denotes the FVS scheme where the velocity splitting functions $V^{\pm}$ have been replaced by $\tilde{V}^{\pm}$ in the convective flux part as described by (48) and (49), together with weighting functions χ_L, χ_R given by (56). Similarly, AUSMD is the Van Leer scheme where $\tilde{V}^{\pm}$ together with (56) have replaced the original splitting functions $V^{\pm}$.

Remark 5. Many choices for the weighting functions χ_L, χ_R can be made such that (53) holds. While our choice (56) works for the present isothermal two-phase model, a more sophisticated choice, where more conditions are imposed, must be made for the nonisothermal case. However, such modifications should be possible to obtain by combining the above approach with ideas previously used for Euler equations [24].

7. MORE NUMERICAL EXPERIMENTS

In this section we revisit the two flow cases we studied in Sections 4.2 and 4.3 and investigate the performance of the two hybrid FVS/FDS schemes denoted as AUSMD and AUSMV. In addition, we do some further testing of AUSMV.

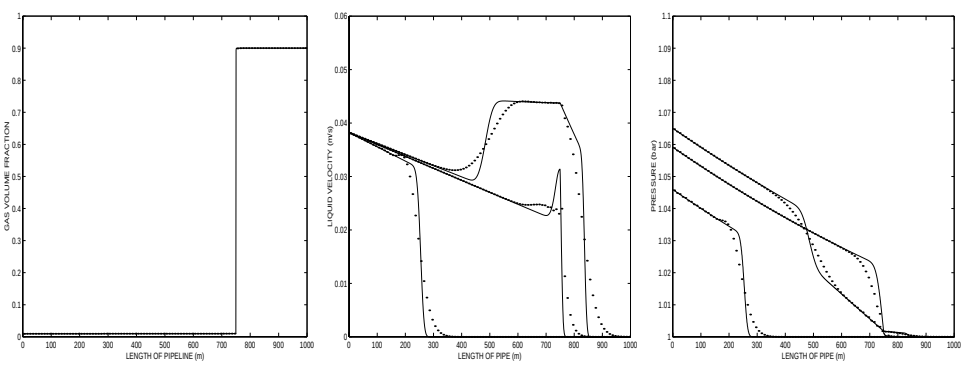

FIG. 15. First-order AUSMV. Left: Gas volume fraction after $t = 7.5$ s. Middle: Liquid velocity. Right: Pressure. The plots of liquid velocity and pressure are considered after $t = 2.5$, 7.5, and 10.0 s.

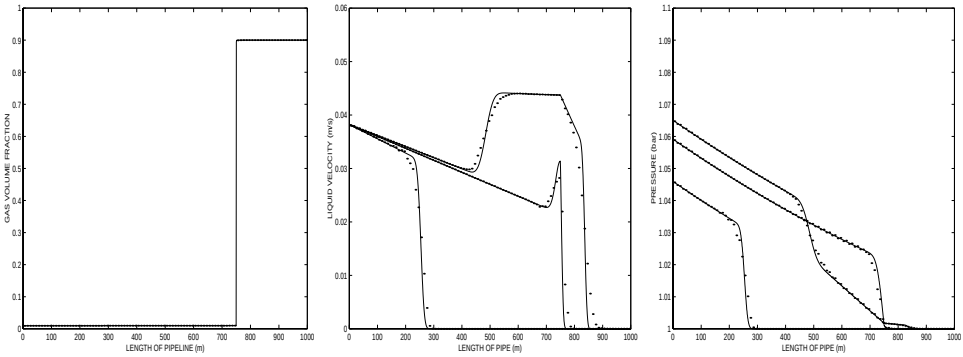

FIG. 16. Second-order AUSMV. Left: Gas volume fraction after $t = 7.5$ s. Middle: Liquid velocity. Right: Pressure. The plots of liquid velocity and pressure are considered after $t = 2.5$, 7.5, and 10.0 s.

7.1. *Fast Transients*

Figure 14 shows the performance of AUSMD for the fast transient flow case. In particular, we see that AUSMD has vanishing dissipation for the stationary gas volume fraction contact discontinuity, similar to AUSM, see Fig. 6. However, severe oscillations (though slightly weaker than for AUSM) are introduced in liquid velocity and pressure, demonstrating that the dissipation provided in AUSMD is not strong enough to ensure a steady shock structure for this flow case.

The necessity of an FVS type of dissipation mechanism to ensure a steady shock structure for the pressure pulse example is demonstrated in Fig. 15. The plots show that the first-order AUSMV scheme is able to capture the velocity and pressure waves in a monotone and accurate way (a minor overshoot is observed at time $t = 2.5$) before the moving sonic waves enter the gas-dominated region at $x = 750$ m as well as after that, when reflecting waves are produced. The performance of the second-order AUSMV is shown in Fig. 16. The success of AUSMV is due to the fact that the scheme has a FVS type dissipation mechanism which keeps a steady shock structure as well as a vanishing dissipation at the stationary gas volume fraction contact discontinuity.

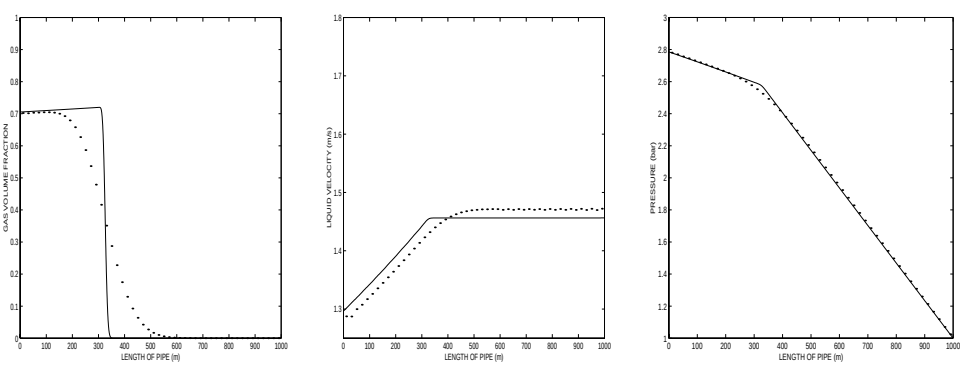

FIG. 17. First-order AUSMD. Left: Gas volume fraction. Middle: Liquid velocity. Right: Pressure. The plots are considered after $t = 250$ s.

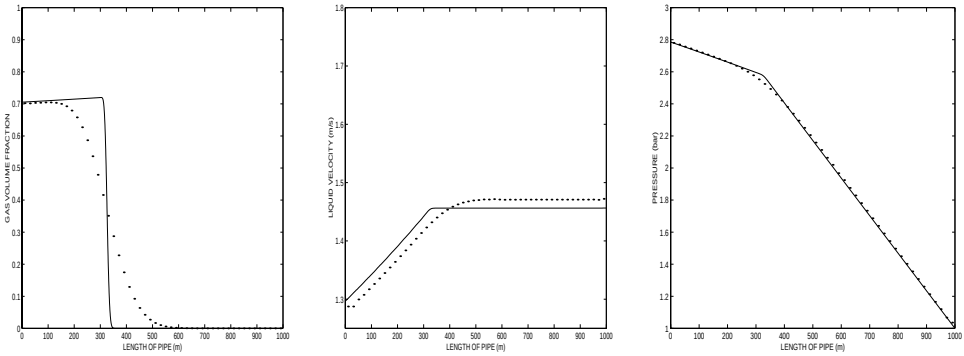

FIG. 18. First-order AUSMV. Left: Gas volume fraction. Middle: Liquid velocity. Right: Pressure. The plots are considered after $t = 250$ s.

7.2. *Slow Transients*

The first- and second-order AUSMD (Figs. 17 and 19) and AUSMV (Figs. 18 and 20) give results that are very similar. Most notably, they both remove the excessive smearing of the moving gas volume fraction contact discontinuity associated with the FVS and Van Leer schemes. Both AUSMD and AUSMV produce results comparable with those of AUSM; compare with Figs. 10 and 13.

7.3. *Comparison between AUSMV and a Roe Scheme*

The objective of the following numerical test is to gain more insight into the approximation properties of the AUSMV scheme. For that purpose, we compare the performance of the first-order AUSMV with that of the first-order of a fully numerical Roe solver. This Roe scheme has previously been tested for the current two-phase model [11, 17]. The Roe scheme is known to be very accurate in the resolution of contact discontinuities. All the presented results have been achieved using the same flow conditions as given in Sections 4.2 and 4.3.

Figure 21 shows the comparison between the first-order AUSMV and the Roe scheme for the pressure pulse example of Section 4.2, where we used a fine grid $\Delta x = 1.0$ m. Figure 22 shows the comparison between the first-order AUSMV and the Roe scheme for the mass

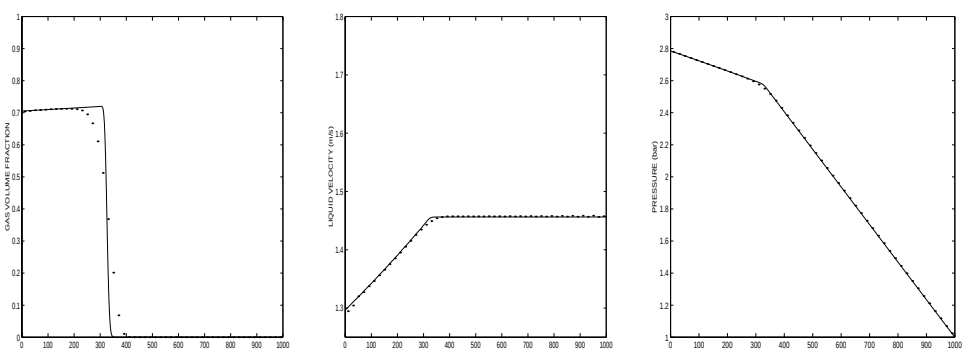

FIG. 19. Second-order AUSMD. Left: Gas volume fraction. Middle: Liquid velocity. Right: Pressure. The plots are considered after $t = 250$ s.

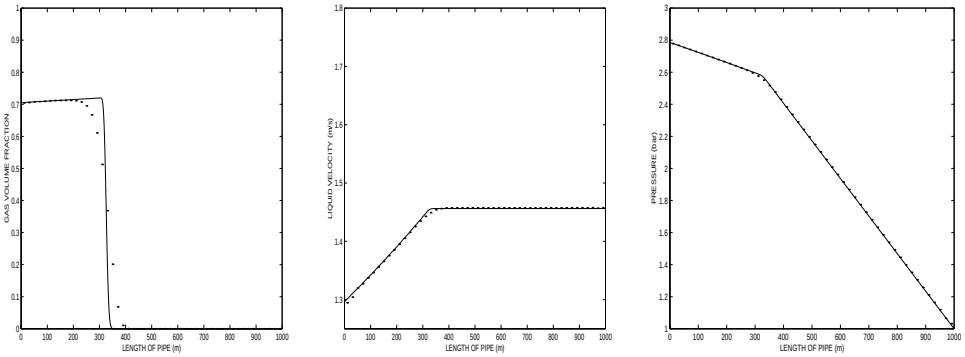

FIG. 20. Second-order AUSMV. Left: Gas volume fraction. Middle: Liquid velocity. Right: Pressure. The plots are considered after $t = 250$ s.

transport example of Section 4.3 using a fine grid $\Delta x = 2.5$ m. The results produced by the two schemes are in very good agreement. In particular, the results indicate that the AUSMV scheme is comparable with the much more expensive fully numerical Roe scheme with respect to accuracy. This test also justifies our use of the AUSMV scheme to generate reference solutions for the flow cases presented in this paper.

7.4. *Flow with Unequal Phase Velocity*

The objective of this numerical example is twofold. First, we want to check the performance of AUSMV on a mass transport example involving unequal fluid velocities. Second, we want to demonstrate that AUSMV works well using only a rough estimate of the two-phase sound velocity ω given by

$$\omega^2 = \frac{p}{\alpha_g \rho_l (1 - \alpha_g)}, \tag{57}$$

which is the sound velocity corresponding to the equal phase velocity model ($K = 1$, $S = 0$).

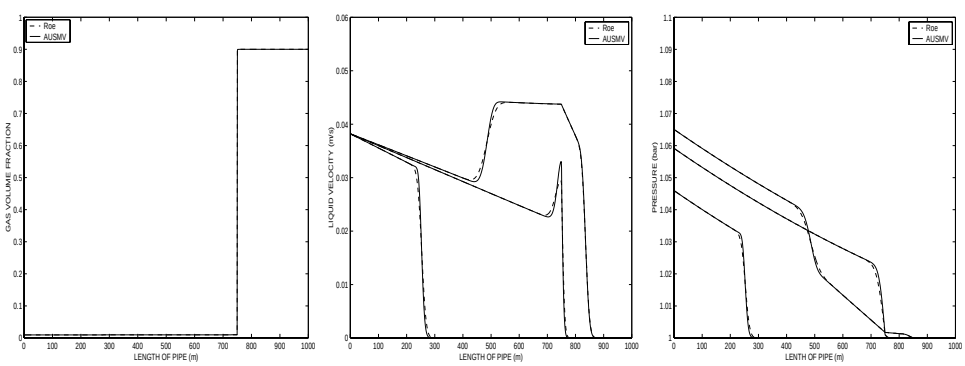

FIG. 21. Comparison of AUSMV and Roe (first order). Left: Gas volume fraction at time $t = 7.5$ s. Middle: Liquid velocity. Right: Pressure. The plots of liquid velocity and pressure are considered after $t = 2.5$, 7.5, and 10.0 s; $\Delta x = 1.0$ m.

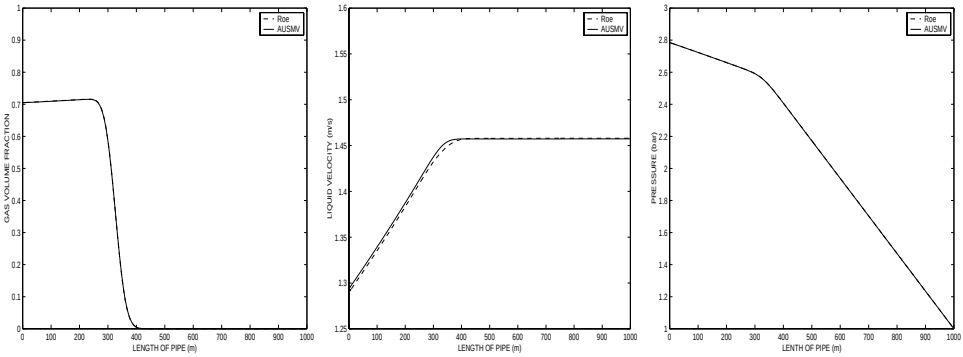

FIG. 22. Comparison of AUSMV and Roe (first order). Left: Gas volume fraction. Middle: Liquid velocity. Right: Pressure. The plots are considered after $t = 250$ s; $\Delta x = 2.5$ m.

We consider the mass transport example of Section 4.3 using the slip (5) with $K = 1.2$ and $S = 0.5$. First, we solved with AUSMV, using (26) together with (13) to estimate the sound velocity for the two-phase mixture. The solutions are shown in Fig. 23. Then we computed the solution with AUSMV using (57) in (26). We observed no difference between these two approximations, and we have not plotted the results of this last computation.

This indicates that we might replace the slip law (5) by a more general hydrodynamic model which determines the slip between the fluid velocities, while still using the no-slip sound velocity ω given by (57) to obtain a rough estimate for the sound velocity to be used in the AUSMV scheme.

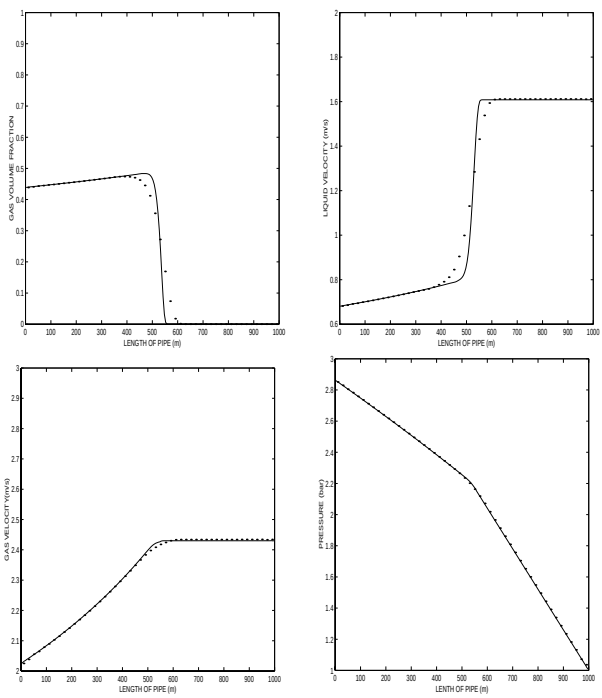

FIG. 23. Second-order AUSMV. Top: Gas volume fraction (left); liquid velocity (right). Bottom: Gas velocity (left); pressure (right). The plots are considered after $t = 250$ s.

8. CONCLUSION

In this paper we have explored different flux-splitting schemes, based on the idea of combining flux-vector splitting (FVS) and flux-difference splitting (FDS), for a one-dimensional two-phase model for unsteady compressible liquid and gas flow. This model is more complex than the Euler equations since the flux cannot be expressed in terms of its conservative variables, hence Jacobians must be calculated numerically, which leads to time-consuming algorithms. This makes it attractive to use methods based on scalar calculations such as flux-vector-splitting schemes. In particular, we propose an FVS, a Van Leer, and an AUSM type scheme by considering natural extensions of ideas applied for Euler equations. We have demonstrated that the FVS scheme is able to capture fast-propagating acoustic waves in pressure and fluid velocity, while it strongly smears volume fraction contact discontinuities. On the other hand, the AUSM type scheme gives accurate resolution of such volume fraction contact discontinuities, while it cannot produce monotone approximations of fast sonic waves in pressure and fluid velocity. In particular, we have proposed a hybrid FVS/FDS scheme, denoted as AUSMV, which combines AUSM and FVS such that accurate solutions are obtained both for fast-moving sonic waves and contact discontinuities. Based on our investigations, we believe that such a hybrid scheme has the potential to become a suitable tool to describe various transport problems described by the current two-phase model. Furthermore, we also believe that ideas presented in this paper can be extended to more general two-fluid models. Such investigations are now in progress.

ACKNOWLEDGMENTS

The first author thanks the Norwegian Research Council for financial support through the PetroForsk program. The authors also thank the referees for their valuable remarks which led to substantial improvement of the first version of this paper.

REFERENCES

1. S. Benzoni-Gavage, *Analyse Numerique des Modeles Hydrodynamiques d'Ecoulements Diphasique Instationnaires dans les Reseaux de Production Petroliere*, Thesis (ENS Lyon, France, 1991).
2. F. Bouchut, Y. Brenier, J. Cortes, and J.-F. Ripoll, A hierarchy of models for two-phase flows, *J. Nonlinear Sci.* **10**, 639 (2000).
3. F. Coquel, K. El Amine, E. Godlewski, B. Perthame, and P. Rascle, A numerical method using upwind scheme for the resolution of two-phase flows, *J. Comput. Phys.* **136**, 272 (1997).
4. J. Cortes, An asymptotic two-fluid model for Roe-scheme computation, in *Computational Fluid Dynamics, Proceedings of ECCOMAS 98* (Wiley, New York, 1998), Vol. 2, pp. 416–420.
5. J. Cortes, A. Debussche, and I. Toumi. A density perturbation method to study the eigenstructure of two-phase flow equation systems, *J. Comput. Phys.* **147**, 463 (1998).
6. J. M. Delhaye, M. Giot, and M. L. Riethmuller, *Thermohydraulics of Two-Phase Systems for Industrial Design and Nuclear Engineering*, (Von Karman Institute, McGraw-Hill, New York, 1981).
7. J. R. Edwards, A low-diffusion flux-splitting scheme for Navier–Stokes calculations, *Comput. Fluids* **26**, 635 (1997).
8. S. Evje and K.-K. Fjelde, *A Controlled Variation Scheme (CVS) for Simulation of Two-Phase Flow*, RF Report 205 (RF-Rogaland Research, Bergen, Norway, 2001).
9. I. Faille and E. Heintze, A rough finite volume scheme for modeling two-phase flow in a pipeline, *Comput. Fluids* **28**, 213 (1999).

10. K.-K. Fjelde, *Numerical Schemes for Complex Nonlinear Hyperbolic Systems of Equations*, Doctoral thesis (University of Bergen, Norway, 2000).
11. K.-K. Fjelde and K.-H. Karlsen, High-resolution hybrid primitive-conservative upwind schemes for the drift flux model, *Comput. Fluids*, to appear.
12. A. Kumbaro and I. Toumi, An approximate linearized Riemann solver for a two-fluid model, *J. Comput. Phys.* **124**, 286 (1996).
13. M. Ishii, *Thermo-Fluid Dynamic Theory of Two-Phase Flow* (Eyrolles, Paris, 1975).
14. M.-S. Liou, A sequel to AUSM: AUSM(+), *J. Comput. Phys.* **129**, 364 (1996).
15. J. M. Masella, I. Faille, and T. Gallouet, On an approximate Godunov scheme, *Int. J. Comput. Fluid Dyn.* **12**, 133–149 (1999).
16. R. B. Pember, Numerical methods for hyperbolic conservation laws with stiff relaxation. I. Spurious solutions, *SIAM J. Appl. Math.* **53**, 1293–1330 (1993).
17. J. E. Romate, An approximate Riemann solver for a two-phase flow model with numerically given slip relation, *Comput. Fluid* **27**, 455 (1998).
18. R. Saurel and R. Abgrall, A multiphase Godunov method for compressible multifluid and multiphase flows, *J. Comput. Phys.* **150**, 425 (1999).
19. H. B. Stewart and B. Wendroff, Two-phase flow: Models and methods, *J. Comput. Phys.* **56**, 363 (1984).
20. B. Theron, *Ecoulements diphasique instationnaires en conduite horizontale*, Thesis, (INP Toulouse, France, 1989).
21. I. Tiselj and S. Petelin, Modelling of two-phase flow with second-order accurate scheme, *J. Comput. Phys.* **136**, 503 (1997).
22. I. Toumi, An upwind numerical method for two-fluid two-phase flow models, *Nucl. Sci. Eng.* **123**, 147 (1996).
23. B. Van Leer, Towards the ultimate conservative difference scheme. V. A second-order sequel to Godunov's method, *J. Comput. Phys.* **32**, 101 (1979).
24. Y. Wada M. and M.-S. Liou, An accurate and robust flux splitting scheme for shock and contact discontinuity, *SIAM J. Sci. Comput.* **18**, 633 (1997).